FAST-TIME FILTERING WITH MULTICHANNEL SAR

Luke Rosenberg[a,b,c] and Doug Gray[a,b]

(a) Department of Electrical and Electronic Engineering, University of Adelaide, Australia
(b) Cooperative Research Centre for Sensor, Signal and Information Processing (CSSIP)
(c) Defence, Science and Technology Organisation (DSTO)
luker@eleceng.adelaide.edu.au, dgray@eleceng.adelaide.edu.au

ABSTRACT

Large regions of a Synthetic Aperture Radar (SAR) image can potentially be destroyed by an airborne broadband jammer. Jammer components include both the direct-path and multipath reflections from the ground, known as hot-clutter or terrain scattered interference. Using multiple antennas on a SAR provides spatial degrees of freedom and allows for beamforming to reject the direct-path signal. However, to effectively suppress non-stationary hot-clutter components, fast-time taps from within a pulse have shown to be effective for airborne radar, [1]-[2]. The goal of interference suppression for SAR is to successfully suppress these interferences while not significantly effecting the image quality by blurring, reducing the resolution or raising the side-lobe level. This paper looks at two fast-time STAP algorithms, the Minimum Variance Distortionless Response (MVDR) and the Generalised Sidelobe Canceller (GSC) to study the effect of non-stationary interference suppression for SAR images.

1. INTRODUCTION

Typical SAR imaging is performed with a large offset range and small field of view. Any jammer signal incident outside the main-beam field of view can easily be suppressed with spatial beamforming alone. However, if the jammer signal is incident in the main-beam, the range profile of a target can be nulled and consequent image formation will lead to a blurry final image. The use of derivative constraints to reduce potential signal suppression has shown to be an effective compromise to reduce the interference without compromising the targets range profile, [3].

In addition to this, non-stationary interference from the 'hot-clutter' will cause the training statistics to change from pulse to pulse and traditional slow-time Space Time Adaptive Processing (STAP) techniques [4], will not be effective. Therefore adapting within each pulse is required by exploiting spatial beamforming or combing spatial/fast-time beamforming. Fast-time STAP offers the advantage of exploiting the coherency between the direct-path jammer and other hot-clutter signals to provide improved interference rejection. Both methods will however cause secondary modulations during image formation, similar to that shown by [5]. This paper analyses these techniques for sidelobe and mainlobe jamming in SAR and utilises the derivative constraints for improved final image quality.

2. SYSTEM MODELS AND GEOMETRY

2.1. SAR Signal Model

Consider a SAR travelling along the y-axis, imaging a point in the slant-plane $x \in [X_c - X_0, X_c + X_0]$, $y \in [-Y_0, Y_0]$. The radar transmits a broadband chirp and the received signal $\tilde{s}_n(t, u, x, y)$, is base-banded and sampled for each of the N channels of a linear antenna array with equi-spaced receivers along the azimuth direction. The variables (t, u) represent (fast-time) samples within a pulse and the SAR platform position (slow-time) respectively. As the SAR bandwidth, B (Hz) is much smaller than the carrier frequency, ω_c (rad/s), the SAR signal model can be split into temporal and spatial components and adaptive filtering can occur either before or after range processing.

The spatial delay is given by the time difference between the centre and the n^{th} channel and can be approximated as a function of the SAR position u or equivalently, an angular offset $\theta(u)$.

$$\begin{aligned}\tilde{\tau}_n(u) &= \frac{1}{c}\left[R\left(X_c, u + d_n\right) - R\left(X_c, u\right)\right] \\ &\approx -\frac{d_n}{c}\sin\underbrace{\left[\arctan(u/X_c)\right]}_{\theta(u)}\end{aligned} \tag{1}$$

where c is the speed of light, $R(\cdot)$ is the radial distance given by Pythagoras and $d_n = n\delta$ is the antenna offset from the array phase centre with antenna spacing δ and $n \in [-(N-1)/2, (N-1)/2]$ for N (odd) antenna elements. The spatial steering vector can then be written as,

$$s_n(u) = \exp\left[-j\omega_c\tilde{\tau}_n(u)\right] \tag{2}$$

The total ground return for the SAR is the integral over all scatterers with radar cross section $f(x, y)$,

$$\gamma_n(t, u) = \int_y\int_x f(x, y)\tilde{s}_n(t, u, x, y)dxdy. \tag{3}$$

Also, if the SAR is being jammed by an airborne platform, there will be an extra signal component required in the data model to represent the direct-path and the ground reflected path (hot-clutter), $z_n(\cdot)$. These signals with the addition of receiver noise $\nu(\cdot)$, form the components seen by the SAR.[1]

$$x_n(t,u) = \gamma_n(t,u) + z_n(t,u) + \nu_n(t,u). \tag{4}$$

The noise signal $\nu_n(\cdot)$ represents the receiver noise for each channel. It is modelled as white Gaussian noise with zero mean and unity variance. Figure 1 shows the processing chain from transmission of the chirp signal, formation of the signal $x_n(t,u)$, range processing, adaption and image formation.

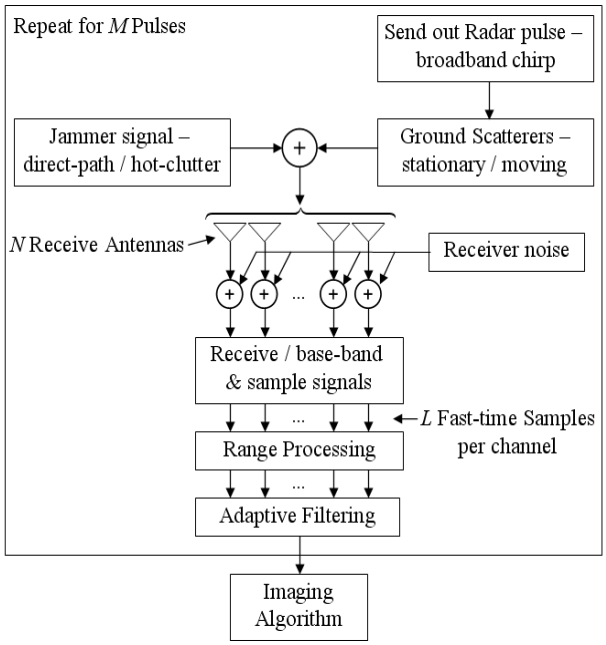

Figure 1: SAR Processing Diagram

2.2. Jammer model

The bistatic jammer model assumes there are K hot-clutter patches within a given area. If an absolute time variable, $\tilde{t} = u/v_p + t$ is defined as the sum of slow-time and fast-time, then the output of the n^{th} receiver, $z_n(\cdot)$, is the superposition of the direct path and the hot-clutter scatterers,

$$z_n(t,u) = \sum_{k=0}^{K} b_k J(\tilde{t} - \tilde{\tau}_{n,k}(t,u)) \tag{5}$$

where $J(\cdot)$ is the jamming signal waveform, $\tilde{\tau}_{n,k}(\cdot)$ is the bistatic delay and b_k is defined as the relative magnitude between the direct-path signal and the jammer signal reflected by the k^{th} scatterer. The zero index refers to the direct-path with $b_0 = 1$.

[1]Note: If there were moving targets in the scene, these would be additional components.

The power spectral density of the jammer signal has a bandwidth $B \ll \omega_c$, centred at baseband. Although the jammer bandwidth is greater than the SAR bandwidth, the received signal is filtered within the receiver to match the SAR bandwidth. Realisations of the jammer signal $J(\cdot)$ can be created from the Inverse Fourier Transform of this signal or autocorrelation,

$$r_J(\tau) = \mathrm{sinc}(B\tau) \tag{6}$$

A physically based model for the multipath scattering is presented by Beckman, [6] and used by [7]. It uses a flat-earth approximation and is referred to as a glistening surface. Using this model, a surface roughness parameter K_β defines the scattering distribution between the SAR and an airborne jammer at heights h_P and h_J respectively, separated by a distance $\tilde{x}_J$ in the ground plane. The scatterer positions are projected onto the slant plane to fit our simulation model and rotated by θ_J according to the jammer position. The coefficients, $b_k = \rho B_k$ for $k > 1$ are formed with a scaling factor ρ, relative to the direct-path and a random magnitude B_k, determined from the scattering model.

The degree of diffuseness from the hot-clutter will greatly effect the final image quality. For example, a high K_β will cause the hot-clutter reflections to be specular and it will appear spatially that only one jamming source is present. However, when K_β is low, the diffuseness is large and the hot-clutter will spread in angle, giving the appearance of a number of different jammer sources incident on the SAR.

The real beampattern for five antenna elements is shown in Figure 2. If the direct-path jammer signal is incident in the mainlobe, the jammer scenario is defined as mainlobe jamming. Correspondingly, for a direct-path jammer signal outside the mainlobe, the jammer scenario is defined as sidelobe jamming. The jammer itself will also have an antenna characteristic with a mainlobe and sidelobes. To emulate this, for each direct-path signal incident on the SAR at θ_J relative to broadside, there will be energy from the sidelobes of the jammer at $\theta_J \pm \theta_{SL}$.

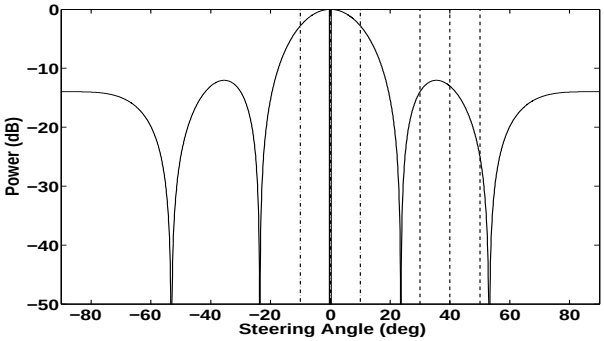

Figure 2: Array Beampattern for $N = 5$, $\theta_{SL} = 10^o$, (–) SAR Field of View, (-.-) Mainlobe Jamming, $\theta_J = 0^o$, (- -) Sidelobe Jamming, $\theta_J = 40^o$

3. FAST-TIME FILTERING

Spatial beamforming requires stacking both the received data and the signal model to form spatial vectors for the l^{th} fast-time range bin with $l = 1 \dots L$ and $t_l = l\Delta t$,

$$\mathbf{x}(l,u) = [x_1(t_l,u), x_2(t_l,u), \dots, x_N(t_l,u)]^T \in \mathcal{C}^{N\times 1},$$
$$\mathbf{s}(u) = [s_1(u), s_2(u), \dots, s_N(u)]^T \in \mathcal{C}^{N\times 1}$$

Conventional beamforming is then performed by matching the received data vector with the spatial steering vector,

$$y(t_l,u) = \mathbf{s}(u)^H \mathbf{x}(l,u) \tag{7}$$

To extend the processing to use fast-time taps, the spatial data vector is stacked over the past $\tilde{L} < L$ fast-time taps,

$$\mathbf{X}(l,u) = \Big[\mathbf{x}(l,u), \mathbf{x}(l-1,u), \dots, \mathbf{x}(l-\tilde{L}+1,u)\Big]^T \in \mathcal{C}^{\tilde{L}N\times 1}$$

with data components for $l < \tilde{L}$ set to zero. Note that in this formulation for fast-time filtering, range ambiguities have been ignored. The corresponding fast-time reference vector is formed by setting the spatial vector at the first block and zeros for the remainder,

$$\mathbf{S}(u) = \mathbf{e}_1 \otimes \mathbf{s}(u) \in \mathcal{C}^{\tilde{L}N\times 1} \tag{8}$$

where $\mathbf{e}_q$ is an $\tilde{L} \times 1$ unit vector with zeros in all positions except for the q^{th} element, which is unity. This form for the fast-time steering vector is used post range processing and assumes the signal of interest is located at the first range gate with negligible range sidelobes. It is also used to maintain the phase of the target signal.

3.1. Adaptive Filtering with Constraints

If the focussing vector in Equation 7 is replaced with a weighted vector, than spatial only adaptive processing can be performed,

$$\tilde{y}(t_l,u) = \mathbf{w}^H(u)\mathbf{x}(l,u) \tag{9}$$

These weights are typically chosen to minimise the mean squared value of the output power subject to to a set of constraints, i.e.

$$\min_{\mathbf{w}(u)} E\{|\mathbf{w}^H(u)\mathbf{x}(l,u)|^2\} \;\text{ subject to }\; \mathbf{C}^H(u)\mathbf{w}(u) = \mathbf{d}$$

where columns of $\mathbf{C}(u)$ describe constraint conditions and $\mathbf{d}$ is the desired responses of the N_{con} constraints. The constrained optimisation problem is solved using Lagrange multipliers to find the weight vector,

$$\mathbf{w}(u) = \mathbf{R}^{-1}(u)\mathbf{C}(u)\Big[\mathbf{C}^H(u)\mathbf{R}^{-1}(u)\mathbf{C}(u)\Big]^{-1}\mathbf{d} \in \mathcal{C}^{N\times 1}$$

where $\mathbf{R}(u)$ is the spatial interference plus noise covariance matrix. The most common constraint on the weight vector is constraining the look direction to be unity by substituting

$$\mathbf{C}(u) = \mathbf{s}(u) \;\;;\;\; \mathbf{d} = 1 \tag{10}$$

into the previous equation. This processor is known as the Minimum Variance Distortionless Response (MVDR) and provides good interference cancellation with sharp nulls in each interference direction.

If the adaption is too strong and the target signal is being modulated, extra constraints can be added to prevent potential signal suppression. One common method is to constrain the first derivative to be zero in the steering direction. In this case, the derivative constraint is given by,

$$\mathbf{C}(u) = \left[\mathbf{s}(u), \frac{\partial \mathbf{s}(u)}{\partial\theta(u)}\right]^T \;\;;\;\; \mathbf{d} = [1,0]^T \tag{11}$$

with,

$$\frac{\partial s_n(u)}{\partial\theta(u)} = s_n(u)\left[-j\omega_c\frac{d_n}{c}\cos[\theta(u)]\right]$$

Fast-time Extension

The fast-time equivalent of Equation 9 is known as an element space implementation and is given by,

$$\tilde{y}(t_l,u) = \mathbf{W}^H(u)\mathbf{X}(l,u) \tag{12}$$

where the constrained optimisation problem and solution are identical but for fast-time vectors instead of spatial ones,

$$\mathbf{W}(u) = \mathbf{R}_{\text{f}}^{-1}(u)\mathbf{C}_{\text{f}}(u)\Big[\mathbf{C}_{\text{f}}^H(u)\mathbf{R}_{\text{f}}^{-1}(u)\mathbf{C}_{\text{f}}(u)\Big]^{-1}\mathbf{d}_{\text{f}} \in \mathcal{C}^{\tilde{L}N\times 1}$$

The space/fast-time covariance matrix is given by $\mathbf{R}_{\text{f}}(u)$ and the fast-time constraint matrix by,

$$\mathbf{C}_{\text{f}}(u) = \mathbf{I}_{\tilde{L}} \otimes \mathbf{C}(u) \in \mathcal{C}^{\tilde{L}N\times\tilde{L}N_{\text{con}}} \tag{13}$$

with corresponding desired response vector,

$$\mathbf{d}_{\text{f}}(u) = \mathbf{e}_1 \otimes \mathbf{d} \in \mathcal{C}^{\tilde{L}N_{\text{con}}\times 1} \tag{14}$$

3.2. Generalised Sidelobe Canceller

An alternative beam space implementation is known as the Generalised Sidelobe Canceller (GSC) and is shown in Figure 3. It forms a set of 'beams' with the main beam in the 'desired' target direction and the other 'reference' beams going through a blocking matrix $\mathbf{B}(u)$ to remove the desired signal from the data. This signal then goes through an adaptive filter to minimise the output power, before being subtracted from the main beam. While the MVDR method relies on constraints to let the target signal through, the GSC is formulated to keep its main beam fixed on the target signal. Also due to the loss of N_{con} degrees of freedom in the adaption, less training data is required for the same adaptive performance. The most important difference however is its behaviour with steering errors, which is superior to the element space adaptive processor previously presented, [8].

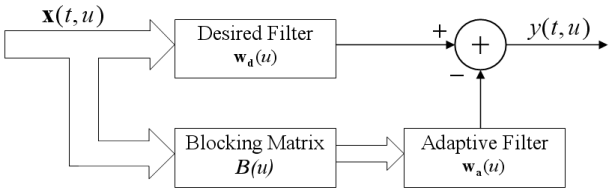

Figure 3: Generalised Sidelobe Canceller

The canceller's output is given by

$$\begin{aligned} y(t,u) &= \mathbf{w}_{\mathrm{d}}^{H}(u)\mathbf{x}(t,u) - \mathbf{w}_{\mathrm{a}}^{H}(u)\mathbf{B}^{H}(u)\mathbf{x}(t,u) \\ &= \left[\mathbf{w}_{\mathrm{d}}(u) - \mathbf{B}(u)\mathbf{w}_{\mathrm{a}}(u)\right]^{H}\mathbf{x}(t,u) \end{aligned} \tag{15}$$

where the desired weight $\mathbf{w}_{\mathrm{d}}(u)$, is given by

$$\mathbf{w}_{\mathrm{d}}(u) = \mathbf{C}(u)\left[\mathbf{C}^{H}(u)\mathbf{C}(u)\right]^{-1}\mathbf{d} \in \mathcal{C}^{N\times 1} \tag{16}$$

The adaptive weight vector $\mathbf{w}_{\mathrm{a}}(u)$, is designed to minimise the output power by solving the unconstrained optimisation [9],

$$\min_{\mathbf{w}_{\mathrm{a}}} \left[\mathbf{w}_{\mathrm{d}}(u) - \mathbf{B}(u)\mathbf{w}_{\mathrm{a}}(u)\right]^{H}\mathbf{R}(u)\left[\mathbf{w}_{\mathrm{d}}(u) - \mathbf{B}(u)\mathbf{w}_{\mathrm{a}}(u)\right],$$

$$\mathbf{w}_{\mathrm{a}}(u) = [\mathbf{B}^{H}(u)\mathbf{R}(u)\mathbf{B}(u)]^{-1}\mathbf{B}^{H}(u)\mathbf{R}(u)\mathbf{w}_{\mathrm{d}}(u) \in \mathcal{C}^{(N-N_{\mathrm{con}})\times 1}$$

To remove the desired signal, the blocking matrix must be orthogonal to the constraint matrix, $\mathbf{B}^{H}(u)\mathbf{C}(u) = 0$. It is designed so each column is a shifted version of a single orthogonal vector of size $N \times (N_{\mathrm{con}} - 1)$ with $N_{\mathrm{con}} + 1$ non-zero elements. Using the Moore-Penrose Pseudo Inverse, [10] a suitable constraint matrix $\mathbf{A}(u)$ can be formed as the concatenation of $N - N_{\mathrm{con}} - 1$ unit vectors with the constraint matrix $\mathbf{C}(u)$. The unit vectors are used to define the position of zeros within the blocking matrix,

$$\mathbf{A}(u) = [\mathbf{e}_{N_{\mathrm{con}}+1} \cdots \mathbf{e}_{N} | \mathbf{C}(u)] \in \mathcal{C}^{N\times(N-N_{\mathrm{con}})} \tag{17}$$

with the Moore-Penrose Pseudo Inverse,

$$\mathbf{A}^{\dagger}(u) = [\mathbf{A}^{H}(u)\mathbf{A}(u)]^{-1}\mathbf{A}^{H}(u) \in \mathcal{C}^{(N-N_{\mathrm{con}})\times N} \tag{18}$$

The first orthogonal column of the blocking matrix is then

$$\begin{aligned} \mathbf{b}(u) &= \mathbf{I}_{N} - \mathbf{A}(u)\mathbf{A}^{\dagger}(u) \\ &= [\tilde{\mathbf{b}}^{T}(u) | \mathbf{0}_{N-N_{\mathrm{con}}-1}^{T}]^{T} \in \mathcal{C}^{N\times 1} \end{aligned} \tag{19}$$

where $\tilde{\mathbf{b}}(u)$ contains $N_{\mathrm{con}} + 1$ non-zero elements and $\mathbf{0}_{N}$ is an $N \times 1$ vector of zeros. The blocking matrix then has the form,

$$\mathbf{B}(u) = \begin{bmatrix} \tilde{\mathbf{b}}(u) & 0 & & 0 & 0 \\ 0 & \tilde{\mathbf{b}}(u) & & 0 & \vdots \\ \vdots & 0 & \ddots & \tilde{\mathbf{b}}(u) & 0 \\ 0 & 0 & & 0 & \tilde{\mathbf{b}}(u) \end{bmatrix} \in \mathcal{C}^{N\times(N-N_{\mathrm{con}})}$$

Fast-time Extension

To extend this algorithm to use $\tilde{L}$ fast-time taps, assume that the target signal is located at the first range gate and the range sidelobes are negligible. The desired fast-time weights are given as,

$$\mathbf{W}_{\mathrm{d}}(u) = \mathbf{e}_{1} \otimes \mathbf{w}_{\mathrm{d}}(u) \in \mathcal{C}^{\tilde{L}N\times 1} \tag{20}$$

with the fast-time blocking matrix expanded similarly to the constraint matrix,

$$\mathbf{B}_{\mathrm{f}}(u) = \mathbf{I}_{\tilde{L}} \otimes \mathbf{B}(u) \in \mathcal{C}^{\tilde{L}N\times\tilde{L}(N-N_{\mathrm{con}})} \tag{21}$$

and the fast-time adaptive weight,

$$\mathbf{W}_{\mathrm{a}}(u) = \left[\mathbf{B}_{\mathrm{f}}^{H}(u)\mathbf{R}_{\mathrm{f}}(u)\mathbf{B}_{\mathrm{f}}(u)\right]^{-1}\mathbf{B}_{\mathrm{f}}^{H}(u)\mathbf{R}_{\mathrm{f}}(u)\mathbf{W}_{\mathrm{d}}(u) \in \mathcal{C}^{\tilde{L}N\times 1}$$

The overall fast-time weight can then be written as,

$$\mathbf{W}(u) = \mathbf{W}_{\mathrm{d}}(u) - \mathbf{B}_{\mathrm{f}}(u)\mathbf{W}_{\mathrm{a}}(u) \in \mathcal{C}^{\tilde{L}N\times 1} \tag{22}$$

3.3. Covariance Matrix

The covariance matrix is estimated by averaging over L_{t} range bins. The space/fast-time covariance $\hat{\mathbf{R}}_{\mathrm{f}}(u)$, then replaces $\mathbf{R}_{\mathrm{f}}(u)$ in the previous algorithms and is known as the sample matrix estimate,

$$\hat{\mathbf{R}}_{\mathrm{f}}(u) = \frac{1}{L_{\mathrm{t}}}\sum_{l=1}^{L_{\mathrm{t}}}\mathbf{Z}(l,u)\mathbf{Z}^{H}(l,u) \in \mathcal{C}^{\tilde{L}N\times\tilde{L}N} \tag{23}$$

It is assumed that techniques as described in [4] can be used to get different realisations of the interference plus noise signal without any targets present. The interference plus noise vector, $\mathbf{Z}(\cdot)$ can then be formed similarly to the data vector $\mathbf{X}(\cdot)$.

4. SIMULATED RESULTS

For the analysis in this paper, a multichannel SAR simulation has been implemented in MATLAB. The parameters chosen are summarised in Table 1 and a comparison between a synthetic SAR 'S' image and the same image with hot-clutter (HC) added is shown in Figure 4. For image formation, a multichannel Spatial Matched Filter / Interpolation algorithm is used [11].

The purpose of this paper is to measure the effect of different constraints on a final SAR image when increasing fast-time taps. Since both element and beam space formulations will produce the same results with no steering errors, only element space results are presented here.

4.1. Performance Measures

The adaptive performance is measured by the amount of interference energy remaining after cancellation. If $y_{\mathrm{ideal}}(t,u)$ is the output signal prior to image formation with no interference present, then the Residual Interference to Noise Ratio (RINR) is estimated by,

Table 1: Simulation Parameters

Parameters	**Value**
Carrier Frequency (f_c) / Bandwidth (B)	10 / 0.3 GHz
Number of Elements (N) / Spacing (δ)	5 / $\frac{\lambda}{2}$ m
Number of Pulses (M) / Range Bins (L)	100 / 280
Range Centre (X_c) / Clutter Noise Ratio	10 km / 20 dB
Range (Δ_X) / Azimuth Resolution (Δ_Y)	1 / 5 m
PRI (T_{PRI}) / Pulse Length (T_p)	3 ms / 45 μs
Fast-time Sampling (Δt) / Training Size (L_t)	$\frac{1}{2B}$ / $3\tilde{L}N$
SAR Height (h_P) / Jammer Height (h_J)	3 / 3 km
Jam. Offset $(\tilde{x}_J)$ / Jammer Sidelobes (θ_{SL})	50 km / 4 deg
No. HC Scats. (K) / Relative HC Magnitude (ρ)	200 / 0.7
Mainlobe/Sidelobe Angle (θ_J)	0 deg / 40 deg
Diffuse/Specular Jammer Power (σ_J^2)	65 dB / 40 dB

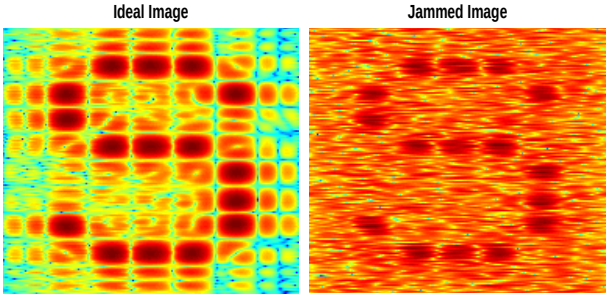

Figure 4: Sample Image - Ideal and with Interference

$$RINR(t,u) = \frac{|y(t,u)|^2}{|y_{\text{ideal}}(t,u)|^2} \tag{24}$$

For comparisons in this paper, the RINR is measured directly after adaption and is averaged over all the range-bins and pulses. A second measure of performance is the Signal Distortion Ratio (SDR) post image formation. Let $Y(x_f, y_g)$ denote the adapted images for pixels $f = 1 \dots F$, $g = 1 \dots G$. Correspondingly, let $D(x_f, y_g)$ denote the ideal image with no jammer added. The SDR is then estimated as

$$SDR = \frac{\sum_{f,g} |D(x_f, y_g)|^2}{\sum_{f,g} |Y(x_f, y_g) - D(x_f, y_g)|^2} \tag{25}$$

4.2. Sidelobe Jamming

Sidelobe jamming isn't as hard to suppress as the mainlobe case since the steering directions are not in the same region as the interference. For this reason there will be little difference with the addition of fast-time taps except with the most diffuse scenario. Comparisons for the MVDR, MVDR with derivative constraint and the conventional processor are presented in Figures 5 to 7.

The three simulation scenarios each have a different total amount of interference. The very diffuse scenario shows a 15-20dB reduction of the interference with respect to the conventional RINR, while this increases to 40dB for the moderately diffuse and specular scenarios. Increasing fast-time taps in the very diffuse scenario shows an improvement of 4-5dB in the RINR. This is also mirrored with the SDR, where the MVDR algorithm shows the best performance with 15 taps. As the diffuseness becomes less, there is a smaller improvement with using fast-time taps and the derivative constraint algorithm starts to show better SDR than the MVDR. In fact for the specular scenario, the derivative constraint doesn't suppress more interference than the MVDR, but produces an image with 40dB improvement in SDR! This is due to the derivative constraint preventing the target signal from being as suppressed. The moderately diffuse and specular RINR results also show a negative RINR, further confirming that part of the target signal has been suppressed during the adaption.

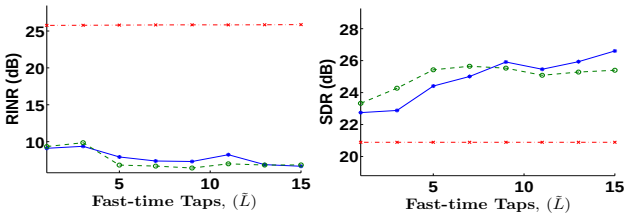

Figure 5: Sidelobe Jamming - $K_\beta = 0.01$ (very diffuse), (—) MVDR, (- -) First Order Deriv., (-.-) Conventional

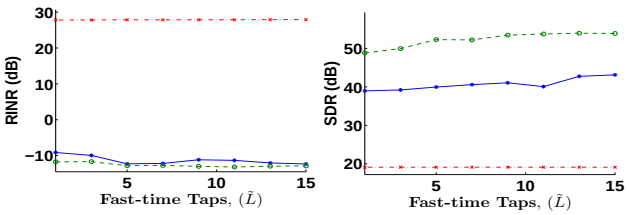

Figure 6: Sidelobe Jamming - $K_\beta = 0.3$ (mod. diffuse), (—) MVDR, (- -) First Order Deriv., (-.-) Conventional

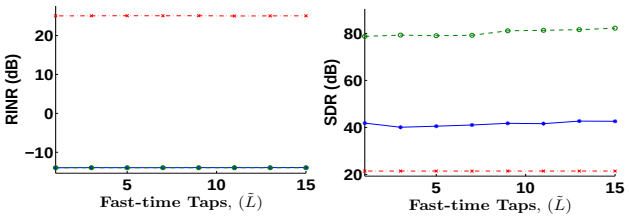

Figure 7: Sidelobe Jamming - $K_\beta = 10$ (specular), (—) MVDR, (- -) First Order Deriv., (-.-) Conventional

4.3. Mainlobe Jamming

Mainlobe jamming is a much harder interference to suppress. Without constraints, the adaptive processor would null the target signal with the interference. However, if the constraint from Equation 10 is imposed for the steering direction, the power from any incident interference signals will instead be minimised. Using derivative constraints to prevent potential signal suppression can therefore be used as a tradeoff to reduce the interference and not significantly

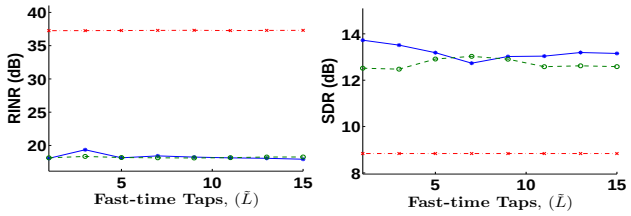

Figure 8: Mainlobe Jamming - $K_\beta = 0.01$ (very diffuse), (—) MVDR, (- -) First Order Deriv., (-.-) Conventional

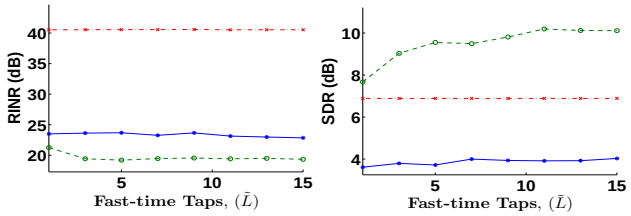

Figure 9: Mainlobe Jamming - $K_\beta = 0.3$ (mod. diffuse), (—) MVDR, (- -) First Order Deriv., (-.-) Conventional

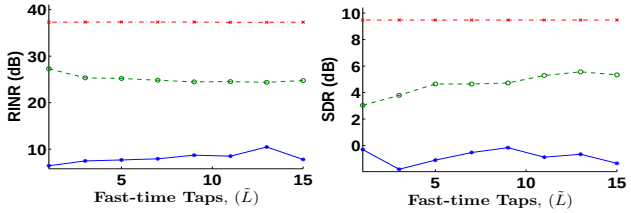

Figure 10: Mainlobe Jamming - $K_\beta = 10$ (specular), (—) MVDR, (- -) First Order Deriv., (-.-) Conventional

modulate the target signals. It is expected that using fast-time taps will increase the performance due to the coherency between the direct-path and other hot-clutter scatterers.

The two diffuse simulation scenarios indicate a 20dB reduction in the RINR, while this increases to 30dB for the specular scenario. Increasing fast-time taps makes little difference for the very diffuse scenario. The MVDR algorithm performs slightly worse, while the derivative constraint performs slightly better.

For the moderately diffuse scenario however, the derivative constraint algorithm shows a 2dB improvement in both RINR and SDR as the number of fast-time taps increase. It is also 3dB above the conventional SDR when it achieves its maximum of 10dB. While both algorithms offer good interference suppression, the MVDR now forms an image which is worse than the conventional one as it is not able to prevent target signal cancellation.

Specular interference in the mainbeam is the toughest to suppress while still maintaining a good quality image. The MVDR algorithm shows the best RINR at a level 17dB below the derivative constraint. With increasing fast-time taps, the derivative constraint algorithm shows a 2dB improvement in SDR and is 6dB above the the MVDR image. However, both algorithms still fall under the conventional SDR level.

5. CONCLUSIONS

Two fast-time implementations of constrained adaptive filtering have been presented with identical results as no steering errors were present in the simulation. In a real system, the beam space GSC algorithm would be preferred over the element-space for its ability to adapt in these situations.

It has been shown that there is a 4-5dB improvement with sidelobe jamming as fast-time taps are used. For the specular case, the first derivative constraint produced a greatly improved SDR over the MVDR algorithm as it was able to prevent the target signal from being as suppressed.

For the mainlobe case, only the moderately diffuse and specular cases show any improvement with increasing fast-time taps. A greater difference however was the moderately diffuse case which showed a 3dB improvement over the conventional SDR, while the specular scenario performed worse than the conventional beamformer! This shows that these algorithms are unable to prevent target signal cancellation while removing a strong specular interference in the main beam.

6. REFERENCES

[1] R. L. Fante and J. A. Torres. Cancellation of Diffuse Jammer Multipath by an Airborne Adaptive Radar. *IEEE Transactions on Aerospace and Electronic Systems*, v31, no. 2, 1995.

[2] R. A. Gabel, S. M. Kogon, and D. J. Rabideau. Algorithms for Mitigating Terrain-Scattered Interference. In *Electronics & Communication Engineering Journal*. Lincoln Labs. MIT, 1999.

[3] L. Rosenberg and D. Gray. Robust Interference Suppression for Synthetic Aperture Radar. *International Symposium on Signal Processing and its Applications*, August 2005.

[4] J. Ward. Space-Time Adaptive Processing for Airborne Radar. Technical report 1015, Lincoln Labs. MIT, 1994.

[5] D. Rabideau. Clutter and Jammer Multipath Cancellation in Airborne Adaptive Radar. *IEEE Proceedings on Aerospace and Electronic Systems*, v36, no. 2, April 2000.

[6] P Beckman. *The Scattering of Electromagnetic Waves from Rough Surfaces*. Pergamon Press Ltd., 1963.

[7] R. L. Fante. Cancellation of Specular and Diffuse Jammer Multipath using a Hybrid Adaptive Array. In *IEEE Transactions on Aerospace and Electronic Systems*. Mitre Corp. Bedford MA USA, 1991.

[8] L.C. Godara. A Robust Adaptive Array Processor. In *IEEE Transactions on Circuits and Systems*, volume 34, no. 7, 1987.

[9] D.H. Johnson and D.E. Dudgeon. *Array Signal Processing - Concepts and Techniques*. Prentice Hall Inc., 1993.

[10] G.H. Golub and C.F. Van Loan. *Matrix Computations, Second Edition*. John Hopkins University Press, 1989.

[11] L. Rosenberg and D. Gray. Multichannel SAR Imaging using Wavefront Reconstruction. In *International Radar Symposium Proceedings*, pages 155–160, 2004.